Available online at www.sciencedirect.com
ScienceDirect
International Journal of Heat and Mass Transfer 50 (2007) 1843–1854
International Journal of HEAT and MASS TRANSFER
www.elsevier.com/locate/ijhmt

Optimal temperature distribution in a 3D triple-layered skin structure embedded with artery and vein vasculature and induced by electromagnetic radiation

Haojie Wang [a], Weizhong Dai [a,*], Adrian Bejan [b]

[a] Mathematics and Statistics, College of Science and Engineering, Louisiana Tech University, Ruston, LA 71272, USA
[b] Department of Mechanical Engineering and Materials Science, Duke University, Durham, NC 27708-0300, USA

Received 15 May 2006; received in revised form 4 October 2006
Available online 28 November 2006

Abstract

In hyperthermia cancer treatments, a crucial problem is keeping the temperature of the normal tissue surrounding the tumor below a certain threshold so as not to cause damage to the tissue. Thus, obtaining a temperature field of the entire treatment region is important to control the process. In this study we develop a model and a numerical method for obtaining an optimal temperature distribution in a triple-layered skin structure embedded with multi-level blood vessels. The heat is induced by electromagnetic (EM) radiation. The dimensions and blood flow of multi-level blood vessels are determined based on the constructal theory.

1. Introduction

Conventional hyperthermia (target temperatures of 42–46 °C) in conjunction with radiation has demonstrated increased effectiveness in the treatment of certain types of cancer, such as skin cancer [1]. The objective is to control heating of the tumor so that the temperature of the normal tissue surrounding the tumor remains low enough so as not to cause damage to the tissue. Hence, for process control, it is important to obtain a temperature field of the entire treatment region. With knowledge of the entire temperature field in the treatment region, clinical personnel can potentially control the heating source to deliver energy to the treatment target volume to raise its minimum temperature above 42 °C, while limiting the temperatures in the normal tissue to prevent damage. However, it is not easy to obtain an accurate determination of the temperature field over the entire treatment region during clinical hyperthermia treatments, because the number of invasive temperature probes that can be used is limited due to the pain tolerance of patients. Furthermore, to ensure that the temperature is within the desired range, the clinician usually monitors the temperature every few seconds by pressing the hold button of the thermocouple needle, and at the same time keeps the thermocouple needle away from the light spot. Thus, it is desirable to develop a mathematical method that can determine the power intensity and the pattern of laser or radiation exposure in order to optimize the temperature distribution in the target region before treatment. In this manner, the treatment efficiency can be assessed more precisely.

Since the determinants of temperature distributions during thermal therapy include the power deposition pattern of the heating source, heat removal by conduction, and heat removal by blood flow forced convection, numerical methods must be developed to solve the bioheat transfer equation in the targeted region [2]. Although

* Corresponding author. Tel.: +1 318 257 3301; fax: +1 318 257 2562.
E-mail address: dai@coes.latech.edu (W. Dai).

0017-9310/$ - see front matter © 2006 Elsevier Ltd. All rights reserved.
doi:10.1016/j.ijheatmasstransfer.2006.10.005

Nomenclature

B_i	Biot number
C_l, C_{b}^l	specific heat of tissue and blood in layer l
C_{B}	heat capacity of blood
c_0	the speed of light in free space
D	electric flux density
E	electric field intensity
F_m	area of cross-section in the mth level vessel
f	frequency of the EM wave
H	magnetic field density
h	heat convection coefficient
k_l	heat conductivity of layer l
L_l	thickness of layer l
L_{b}^m	length of the blood vessel in level m along the flowing direction of blood
M_m	main flow of blood in the mth level vessel
N_x, N_y, N_l^z	numbers of grid points in the x, y, z directions, respectively
NX, NY	lengths of the skin structure in the x, y directions, respectively
$\mathrm{NL}_{\mathrm{b}}^m$, $\mathrm{NW}_{\mathrm{b}}^m$	length and width of the cross-section of the mth level vessel
P	vessel periphery
$\dot{P}$	blood flow rate
Q_{r}^l	heat source in layer l
S	sum of least squares
t	time
u_{ijk}^n	numerical solution of temperature elevation of tissue
u_{b}^m	numerical solution of temperature elevation of blood in the mth level vessel
v_m	velocity of blood flow in the mth level vessel
W_{b}^l	blood perfusion rate in layer l
x, y, z	Cartesian coordinates
δ_x^2, δ_y^2, δ_z^2	second-order finite difference (FD) operators
Δx, Δy, Δz	mesh sizes of FD scheme for bioheat transfer model in the x, y, z directions
Δx, Δy, δz	mesh sizes of finite difference time domain scheme in the x, y, z directions
Δt	time increment used in calculating heat transfer
δt	time increment used in calculating EM wave
ρ_l	density of layer l
θ_{b}^m, θ_l, θ_{w}^m	temperature elevations in blood, tissue, and vessel wall, respectively
θ_{in}, θ_{out}	temperature elevations of blood at entrance and exit, respectively
ε_0	permittivity of free space
μ_0	permeability of free space
$\varepsilon_{\mathrm{r}}^*$	relative dielectric constant
ε_∞	permittivity in the terahertz frequency range
$\Delta\varepsilon$	drop in permittivity in the frequency range
σ_1	ionic conductivity
α_m	adjustable parameter between 0 and 1, $m = 1, 2, 3, 4$
τ	relaxation time
ω	angular frequency

there are many studies on laser, radio-frequency, or micro-wave induced hyperthermia [1–21], the numerical model for electromagnetic-wave induced hyperthermia in triple-layered skin structures composed of epidermis, dermis and subcutaneous embedded with multi-level blood vessels has not been studied. This research is important for certain types of cancer treatment, such as skin cancer.

Recently, we [22,23] have developed a numerical method for obtaining optimal temperature distributions in a 3D triple-layered skin structure embedded with multi-level blood vessels. The heat is induced by a laser and the dimensions and blood flow of the multi-level blood vessels are determined based on the recently developed constructal theory of multi-scale tree-shaped heat exchangers [24–26]. In this article, we extend our research to the case that the heat is induced by electromagnetic radiation. This involves an inverse prediction of the EM wave power input over time in order to control the temperature field so that it is in agreement with a pre-specified temperature required for treatment. The heat generation is calculated based on Maxwell's equations coupled with the Cole–Cole expression [27,28] for the frequency dependence of the dielectric properties of tissue.

2. Model

2.1. Bioheat transfer model

Based on histological knowledge, the largest arteries of the skin are arranged in the form of a flat network in the subcutaneous tissue, immediately below the dermis. The dermis is very sparingly supplied with capillaries and the capillary beds of skin lie immediately under the epidermis [29]. Fig. 1 shows a realistic skin structure configuration.

To simplify our computation, we consider the target region to be a rectangular structure embedded with two countercurrent multi-level blood vessels that cross through the subcutaneous layer from the bottom to the top, as shown in Fig. 2. In this figure, only large blood vessels can be seen in the subcutaneous because the dermis layer consists of only capillaries and the contribution of these small vessels to the heat transfer could be ignored [21].

In Fig. 2, the basic arterial model consists of the large central vessel (level 1) running lengthwise (in the z-direction) along the control volume. This vessel has a horizontal (in the x-direction) vessel (level 2) branching from it. The second vessel goes to third vessel (level 3) which runs again lengthwise (in the z-direction). The second vessel does not

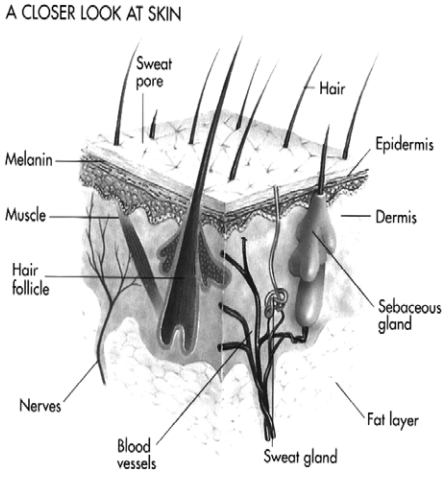

Fig. 1. Skin structure and its components [42].

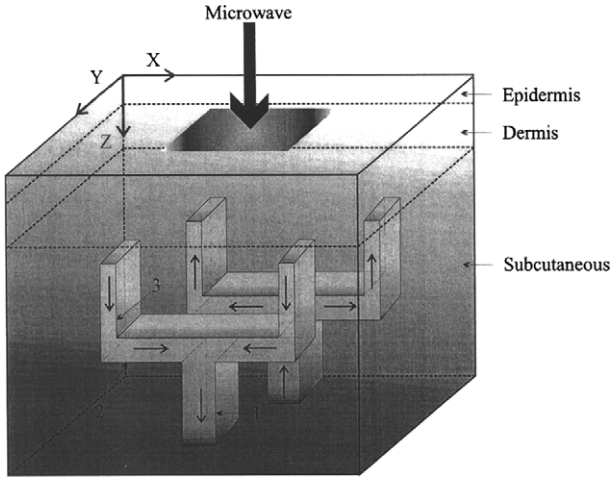

Fig. 2. Configuration of a 3D skin structure.

branch into two third vessels and the diameters of these also are the same, which are similar to those in [6]. These vessels are modeled as slim cuboids for simplicity. The diameters of the arteries are assumed to be decreasing by a constant ratio γ between successive levels of branched vessels, which is given by [25],

$$\gamma = \frac{\mathrm{NL}_\mathrm{b}^2}{\mathrm{NL}_\mathrm{b}^1} = \frac{\mathrm{NW}_\mathrm{b}^2}{\mathrm{NW}_\mathrm{b}^1} = 2^{-\frac{1}{3}}, \tag{1}$$

where NL_b^m and NW_b^m are the length and width of the cross-section of a blood vessel in level m, respectively. The length of blood vessel is assumed to be double after two consecutive construction steps, which can be expressed in the length-doubling rule [26] as follows:

$$L_\mathrm{b}^m = 2^{\frac{1}{2}} L_\mathrm{b}^{m+1}, \quad m = 1, 2, \tag{2}$$

where L_b^m is the length of the blood vessel in level m. The mass flow of blood in the mth level vessel, $M_m = v_m F_m$, is assumed to satisfy [26],

$$M_1 = 2M_2, \quad M_2 = M_3, \tag{3}$$

where v_m is the velocity of blood flow and F_m ($= \mathrm{NL}_\mathrm{b}^m \times \mathrm{NW}_\mathrm{b}^m$) is the area of the cross-section in the mth level vessel.

Furthermore, the temperature elevation of blood in the cross-section of a vessel is assumed to be uniform. We further assume that a steady-state energy balance in the blood vessel can be reached because the length of the considered blood vessel is relatively short and the blood velocity is relatively high. However, one may use a transient heat transfer equation for a more accurate solution. Hence, the convective energy balance equations which are used to calculate the main artery (levels 1 and 2) elevated blood temperatures can be expressed as [7,10]

$$C_\mathrm{B} M_1 \frac{\mathrm{d}(\theta_\mathrm{b}^1)}{\mathrm{d}z} - \alpha P_1 (\theta_\mathrm{w}^1 - \theta_\mathrm{b}^1) = 0 \tag{4}$$

and

$$C_\mathrm{B} M_2 \frac{\mathrm{d}(\theta_\mathrm{b}^2)}{\mathrm{d}x} - \alpha P_2 (\theta_\mathrm{w}^2 - \theta_\mathrm{b}^2) = 0, \tag{5}$$

where C_B is the heat capacity of blood, and α is the heat transfer coefficient between blood and tissue, and P_m is the vessel perimeter. Further, θ_w^m and θ_b^m are the wall temperature elevation and the blood temperature elevation in the mth level vessel. For the smallest, terminal arterial vessels (level 3), a decreased blood flow rate ($\dot{P}$) is included in the energy balance equation [7,10]

$$C_\mathrm{B} M_3 \frac{\mathrm{d}(\theta_\mathrm{b}^3)}{\mathrm{d}z} - \alpha P_3 (\theta_\mathrm{w}^3 - \theta_\mathrm{b}^3) - \dot{P} C_\mathrm{B} F \theta_\mathrm{b}^3 = 0. \tag{6}$$

For simplicity, the venous model is taken to be similar to as the arterial model except that the blood velocity in the vein is opposite to that in the artery to account for the countercurrent flowing in these two kinds of vessels, as shown in Fig. 2. Also, the diameter ratio, length ratio, and mass flow ratio of the blood between the successive levels of the branched veins take the same form as described in Eqs. (1)–(3) for the arteries. Moreover, the convective energy balance Eqs. (4)–(6) used to calculate the blood temperature elevations in the artery domain is applied to the vein domain at the corresponding levels.

The modified Pennes equation that describes the thermal behavior in the triple-layered skin structure when irradiated by the electromagnetic wave can be expressed as follows [30]:

$$\rho_l C_l \frac{\partial \theta_l}{\partial t} + W_\mathrm{b}^l C_\mathrm{b}^l (\theta_l - \theta_\mathrm{out}) - k_l \left[\frac{\partial^2 \theta_l}{\partial x^2} + \frac{\partial^2 \theta_l}{\partial y^2} + \frac{\partial^2 \theta_l}{\partial z^2} \right] = Q_\mathrm{r}^l, \quad l = 1, 2, 3, \tag{7}$$

where θ_l is the tissue temperature elevation due to heating induced by electromagnetic wave; θ_out is the blood temperature elevation at exit or entrance of the third level vessel for the artery or vein respectively; ρ_l, C_l and k_l denote density, specific heat, and thermal conductivity of tissue, respectively; C_b^l is the specific heat of blood; W_b^l is the blood perfusion rate; and Q_r^l is the volumetric heat due to spatial heating.

On the skin surface, we assume that the heat exchange with the surroundings is

$$k_1 \frac{\partial \theta_1}{\partial z} = h(\theta_1 - \theta_{\text{air}}), \quad z = 0. \tag{8}$$

For simplicity, we assume that the heat flux approaches zero as the tissue depth increases, which is realistic for a biological body [31]. The other boundary conditions in the tissue are assumed to be

$$\frac{\partial \theta_l}{\partial \vec{n}} = 0, \tag{9}$$

where $\vec{n}$ is the unit outward normal vector on the boundary. At the entrance to the first level vessel, we have

$$\theta_{\text{b}}^1 = \theta_{\text{in}}, \tag{10}$$

where θ_{in} is the blood temperature elevation at the entrance of the artery. At the exit of the artery, we assume that the blood temperature elevation is equal to the surrounding tissue temperature elevation

$$\theta_{\text{b}}^3 = \theta_{\text{out}}. \tag{11}$$

As mentioned earlier, the velocity of the vein blood has an opposite direction to that of the artery blood. Thus, the entrance of the blood to the vein is located at the third level and the blood temperature elevation is equal to the surrounding tissue temperature elevation.

The continuity of heat transfer between the lateral blood vessel and the tissue requires [32]

$$\frac{\partial \theta_{\text{b}}^m}{\partial \vec{n}} = B_i(\theta_{\text{w}}^m - \theta_{\text{b}}^m). \tag{12}$$

The interfacial continuity between layers are

$$\theta_1 = \theta_2, \quad k_1 \frac{\partial \theta_1}{\partial z} = k_2 \frac{\partial \theta_2}{\partial z}, \quad z = L_1, \tag{13a}$$

$$\theta_2 = \theta_3, \quad k_2 \frac{\partial \theta_2}{\partial z} = k_3 \frac{\partial \theta_3}{\partial z}, \quad z = L_1 + L_2. \tag{13b}$$

The initial condition is

$$\theta_l = 0, \quad t = 0, \ l = 1, 2, 3. \tag{14}$$

2.2. Heat source

The heat source can be obtained based on the electromagnetic fields and the conversion of electromagnetic energy into heat. The distribution of electromagnetic fields in space and time is governed by the "normalized" Maxwell's equations as follows:

$$\frac{\partial \vec{D}}{\partial t} = \frac{1}{\sqrt{\varepsilon_0 \mu_0}} \vec{\nabla} \times \vec{H}, \tag{15}$$

$$\vec{D}(\omega) = \varepsilon_{\text{r}}^*(\omega) \cdot \vec{E}(\omega), \tag{16}$$

$$\frac{\partial \vec{H}}{\partial t} = -\frac{1}{\sqrt{\varepsilon_0 \mu_0}} \vec{\nabla} \times \vec{E}, \tag{17}$$

where $\vec{D}(\omega) = (\frac{1}{\varepsilon_0 \mu_0})^{1/2} \mathbf{D}(\omega)$ is the electric flux density, $\vec{E}(\omega) = (\frac{\varepsilon_0}{\mu_0})^{1/2} \mathbf{E}(\omega)$ is the electric density, $\vec{H}$ is the magnetic density, ε_0 is the permittivity of free space, μ_0 is the permeability of free space, ω is the angular frequency, and $\varepsilon_{\text{r}}^*(\omega)$ is the relative dielectric constant which can be expressed [27,28]:

$$\varepsilon_{\text{r}}^*(\omega) = \varepsilon_\infty + \sum_{m=1}^{4} \frac{\Delta \varepsilon_m}{1 + (\text{j}\omega\tau_m)^{1-\alpha_m}} + \frac{\sigma_1}{\text{j}\omega\varepsilon_0}, \tag{18}$$

where ε_∞ is the permittivity in the terahertz frequency range, σ_1 is the ionic conductivity, and $\text{j} = \sqrt{-1}$; and for each dispersion region m, τ_m is the relaxation time, α_m is an adjustable parameter between 0 and 1, and $\Delta\varepsilon_m$ is the drop in permittivity in the frequency range. Eq. (18), which is called the Cole–Cole expression, is based on the well-known dispersive properties of biological matter and their expression as a summation of terms corresponding to the main polarization mechanisms [33]. The dielectric spectrum extends from Hz to GHz and shows four major regions of dispersion [28]. The complexity of the structure and composition of biological material is such that each dispersion region is broadened by multiple contributions to it and therefore can be described by the Cole–Cole expression. With a choice of parameters appropriate to each tissue, Eq. (18) can be used to predict its dielectric behavior over the desired frequency range [28]. Solving Maxwell's equations coupled with the Cole–Cole expression by using the finite difference time domain (FDTD) method, however, is difficult because it is not easy to convert the equations from the frequency domain to the time domain when $0 < \alpha < 1$.

The dissipated density is the electromagnetic wave energy absorbed in the material. It is eventually converted into thermal energy. The dissipated power density is influenced by the field intensity distribution and electric properties. The heat function, Q_{r}^l, which will be included as a source term in the bioheat transfer equation, Eq. (7), can be expressed as [34]:

$$Q_{\text{r}}^l = \omega\varepsilon_0\varepsilon_{\text{eff}}''|\vec{E}|^2 + \omega\mu_0\mu_{\text{eff}}''|\vec{H}|^2, \tag{19}$$

where $\varepsilon_{\text{eff}}''$ and μ_{eff}'' are relative loss factors related to dipolar, electronic, atomic, space charge and conduction losses. In the case of dielectric materials, there are no magnetic losses and the second term on the right-hand side of the above equation is negligible. In our study, a sinusoidal wave is considered as

$$E_z = E_0 \sin(2\pi f \cdot t), \tag{20}$$

where E_0 is the amplitude of the incident wave, f is the frequency of the wave, and t is time. Consequently, the volumetric heating rate can be computed from peak field amplitudes as [34]

$$Q_{\text{r}}^l = \frac{1}{2}\omega\varepsilon_0\varepsilon_{\text{eff}}''|\vec{E}_{\max}|^2, \tag{21}$$

where $\varepsilon_{\text{eff}}''$ is obtained based on Eq. (18) as follows:

$$\varepsilon''_{\text{eff}} = \sum_{m=1}^{4} \frac{\Delta\varepsilon_m (\omega\tau_m)^{1-\alpha_m} \cos\left(\frac{1}{2}\alpha_m\pi\right)}{1 + 2(\omega\tau_m)^{1-\alpha_m} \sin\left(\frac{1}{2}\alpha_m\pi\right) + (\omega\tau_m)^{2(1-\alpha_m)}} + \frac{\sigma_1}{\omega\varepsilon_0}. \tag{22}$$

3. Numerical method

3.1. Finite difference scheme for bioheat transfer model

The finite difference scheme used for the above bioheat transfer model is similar to that developed in [23]. For the purpose of algorithm description later, we still list the scheme in this section. We denote $(u_l)^n_{ijk}$ and u_b the numerical approximations of (θ_l) $(i\Delta x, j\Delta y, k\Delta z, n\Delta t)$ and θ_b, where Δx, Δy, Δz, and Δt are the spatial and temporal mesh sizes, and i, j, k are integers with $0 \leqslant i \leqslant N_x$, $0 \leqslant j \leqslant N_y$, $0 \leqslant k \leqslant N^z_l$, so that $N_x\Delta\ x = \text{NX}$, $N_y\Delta y = \text{NY}$, and $N^z_l\Delta z = L_l$, $l = 1,2,3$. In this mesh, we assume that $(u_3)^n_{ijk} = (u^m_b)_{ijk}$ when the grid point (i,j,k) is in the mth level blood vessel. Because Eqs. (4)–(6) are first-order ordinary differential equations once θ^m_w is determined, they can be solved by using the fourth-order Runge–Kutta method [35]. Eq. (7) is discretized as follows:

$$\rho_l C_l \frac{(u_l)^{n+1}_{ijk} - (u_l)^n_{ijk}}{\Delta t} + W^l_b C^l_b \left[\frac{(u_l)^{n+1}_{ijk} + (u_l)^n_{ijk}}{2} - (u_b)_{\text{out}}\right] = k_l(\delta^2_x + \delta^2_y + \delta^2_z)\frac{(u_l)^{n+1}_{ijk} + (u_l)^n_{ijk}}{2} + (Q^l_r)^{n+\frac{1}{2}}_{ijk}, \quad l = 1,2,3, \tag{23}$$

where $\delta^2_x u_{ijk} = \frac{u_{i+1jk} - 2u_{ijk} + u_{i-1jk}}{\Delta x^2}$ and so on for the y and z directions. The discrete interfacial equations for Eqs. (13a) and (13b) are assumed to be, for any time level,

$$k_1 \frac{(u_1)^n_{ijN^z_1} - (u_1)^n_{ijN^z_1-1}}{\Delta z} = k_2 \frac{(u_2)^n_{ij1} - (u_2)^n_{ij0}}{\Delta z}, \quad (u_1)^n_{ijN^z_1} = (u_2)^n_{ij0}, \tag{24a}$$

and when the grid point (i,j) is in the tissue

$$k_2 \frac{(u_2)^n_{ijN^z_2} - (u_2)^n_{ijN^z_2-1}}{\Delta z} = k_3 \frac{(u_3)^n_{ij1} - (u_3)^n_{ij0}}{\Delta z}, \quad (u_2)^n_{ijN^z_2} = (u_3)^n_{ij0}. \tag{24b}$$

The interfacial condition, Eq. (12), between the tissue and the lateral blood vessel is discretized as follows:

$$(u_3)^{n+1}_{ijk} = \left[(u_3)^{n+1}_{i+1jk} + Bi\cdot\Delta x\cdot(u_3)^{n+1}_{i-1jk}\right] \Big/ (1 + Bi\cdot\Delta x), \tag{25a}$$

$$(u_3)^{n+1}_{ijk} = \left[(u_3)^{n+1}_{ij+1k} + Bi\cdot\Delta y\cdot(u_3)^{n+1}_{ij-1k}\right] \Big/ (1 + Bi\cdot\Delta y), \tag{25b}$$

$$(u_3)^{n+1}_{ijk} = \left[(u_3)^{n+1}_{ijk+1} + Bi\cdot\Delta z\cdot(u_3)^{n+1}_{ijk-1}\right] \Big/ (1 + Bi\cdot\Delta z), \tag{25c}$$

where the grid point (i, j, k) is on the lateral walls of the blood vessel in the x, y, z directions, respectively. When the grid point (i, j, k) is in the tissue, the initial and other boundary conditions are discretized as follows:

$$(u_l)^0_{ijk} = 0, \tag{26a}$$

$$(u_l)^n_{0jk} = (u_l)^n_{1jk}, \quad (u_l)^n_{N_xjk} = (u_l)^n_{N_x-1jk}, \tag{26b}$$

$$(u_l)^n_{i0k} = (u_l)^n_{i1k}, \quad (u_l)^n_{iN_yk} = (u_l)^n_{iN_y-1k} \tag{26c}$$

$$k_1 \frac{(u_1)^n_{ij1} - (u_1)^n_{ij0}}{\Delta z} = h((u_1)^n_{ij0} - \theta_{\text{air}}), \tag{26d}$$

$$(u_3)^n_{ijN^z_3} = (u_3)^n_{ijN^z_3-1}, \tag{26e}$$

for any time level n.

3.2. Finite difference time domain method for EM fields

Since $\varepsilon^*_r(\omega)$ given by Eq. (18) is a complicated expression, we employ the z-transform described in [36] to simplify the situation. Letting $x(t) = \sum_{n=0}^{\infty} x(n\Delta t)\delta(t - n\Delta t)$, its z-transform is defined as $X(z) = \sum_{n=0}^{\infty} x(n\Delta t)z^{-n} \equiv Z(x(t))$. It can be seen that $Z(x(t - \Delta t)) = z^{-1}X(z)$ (which means that the inverse z-transform of $z^{-1}X(z)$ is $x(t - \Delta t)$), and $j\omega$ can be replaced by $\frac{1-z^{-1}}{\Delta t}$ in the z-transform [36]. Applying the z-transform method to Eq. (16), where $\varepsilon^*_r(\omega)$ is given by Eq. (18), we obtain

$$\vec{D}(z) = \varepsilon_\infty \vec{E}(z) + \frac{\Delta\varepsilon_1 \vec{E}(z)}{1 + \left(\frac{\tau_1}{\Delta t}\right)^{1-\alpha_1}(1 - z^{-1})^{1-\alpha_1}} + \frac{\Delta\varepsilon_2 \vec{E}(z)}{1 + \left(\frac{\tau_2}{\Delta t}\right)^{1-\alpha_2}(1 - z^{-1})^{1-\alpha_2}} + \frac{\Delta\varepsilon_3 \vec{E}(z)}{1 + \left(\frac{\tau_3}{\Delta t}\right)^{1-\alpha_3}(1 - z^{-1})^{1-\alpha_3}} + \frac{\Delta\varepsilon_4 \vec{E}(z)}{1 + \left(\frac{\tau_4}{\Delta t}\right)^{1-\alpha_4}(1 - z^{-1})^{1-\alpha_4}} + \frac{\sigma_1\Delta t}{\varepsilon_0}\cdot\frac{\vec{E}(z)}{1 - z^{-1}}. \tag{27}$$

$\vec{D}(z)$ is very complicated and difficult to transform back to the time domain. This difficulty can be overcome by letting

$$\vec{I}(z) = \frac{\sigma_1\Delta t}{\varepsilon_0}\cdot\frac{\vec{E}(z)}{1 - z^{-1}}, \quad \vec{S}_1(z) = \frac{\Delta\varepsilon_1 \vec{E}(z)}{1 + \left(\frac{\tau_1}{\Delta t}\right)^{1-\alpha_1}(1 - z^{-1})^{1-\alpha_1}}, \tag{28}$$

with similar expressions for $\vec{S}_2(z)$, $\vec{S}_3(z)$ and $\vec{S}_4(z)$. From Eq. (28), we have

$$\vec{I}(z) = \frac{\sigma_1\Delta t}{\varepsilon_0}\vec{E}(z) + z^{-1}\vec{I}(z), \quad \vec{S}_1(z)\left[1 + \left(\frac{\tau_1}{\Delta t}\right)^{1-\alpha_1}(1 - z^{-1})^{1-\alpha_1}\right] = \Delta\varepsilon_1\vec{E}(z). \tag{29}$$

It is noteworthy that if α_1 is not 0 or 1, then powers of z in Eq. (27) are not integers. This complicates determination of the time steps when Eq. (29) is converted back to the time domain. The situation is simplified by employing a second-order Taylor approximation as follows:

$$(1 - z^{-1})^{1-\alpha_1} \approx 1 - (1 - \alpha_1)z^{-1} - \frac{1}{2}(1 - \alpha_1)\alpha_1 z^{-2}. \tag{30}$$

Substituting Eq. (30) into Eq. (29) and rearranging terms, we obtain

$$\vec{S}_1(z) = \frac{\left(\frac{\tau_1}{\Delta t}\right)^{1-\alpha_1}}{1+\left(\frac{\tau_1}{\Delta t}\right)^{1-\alpha_1}}\left[(1-\alpha_1)z^{-1}\vec{S}_1(z) + \frac{1}{2}(1-\alpha_1)\alpha_1 z^{-2}\vec{S}_1(z)\right] + \frac{\Delta\varepsilon_1}{1+\left(\frac{\tau_1}{\Delta t}\right)^{1-\alpha_1}}\vec{E}(z). \tag{31}$$

Similar expressions are obtained for $\vec{S}_2(z)$, $\vec{S}_3(z)$ and $\vec{S}_4(z)$. Substituting these results into Eq. (27), we obtain

$$\vec{D}(z) = A\vec{E}(z) + \sum_{m=1}^{4} B_m\left[(1-\alpha_m)z^{-1}\vec{S}_m(z) + \frac{1}{2}(1-\alpha_m)\alpha_m z^{-2}\vec{S}_m(z)\right] + z^{-1}\vec{I}(z), \tag{32}$$

where

$$A = \varepsilon_\infty + \frac{\sigma_1\Delta t}{\varepsilon_0} + \sum_{m=1}^{4}\frac{\Delta\varepsilon_m}{1+\left(\frac{\tau_m}{\Delta t}\right)^{1-\alpha_m}}, \tag{33}$$

$$\vec{S}_m(z) = B_m\left[(1-\alpha_m)z^{-1}\vec{S}_m(z) + \frac{1}{2}(1-\alpha_m)\alpha_m z^{-2}\vec{S}_m(z)\right] + \frac{\Delta\varepsilon_m}{1+\left(\frac{\tau_m}{\Delta t}\right)^{1-\alpha_m}}, \tag{34}$$

$$B_m = \frac{\left(\frac{\tau_m}{\Delta t}\right)^{1-\alpha_m}}{1+\left(\frac{\tau_m}{\Delta t}\right)^{1-\alpha_m}}, \quad m = 1,2,3,4. \tag{35}$$

Hence, we can transform Eq. (32) back to the time domain and obtain $\vec{E}$ at time step n

$$\vec{E}^n = \frac{1}{A}\left\{\vec{D}^n - \vec{I}^{n-1} - \sum_{m=1}^{4} B_m\left[(1-\alpha_m)\vec{S}_m^{n-1} + \frac{1}{2}(1-\alpha_m)\alpha_m\vec{S}_m^{n-2}\right]\right\}, \tag{36}$$

where $\vec{I}^n$ and $\vec{S}_m^n$ $(m = 1,2,3,4)$ are calculated as follows:

$$\vec{I}^n = \frac{\sigma_1\Delta t}{\varepsilon_0}\vec{E}^n + \vec{I}^{n-1}, \tag{37}$$

$$\vec{S}_m^n = B_m\left[(1-\alpha_m)\vec{S}_m^{n-1} + \frac{1}{2}(1-\alpha_m)\alpha_m\vec{S}_m^{n-2}\right] + \frac{\Delta\varepsilon_m}{1+\left(\frac{\tau_m}{\Delta t}\right)^{1-\alpha_m}}\vec{E}^n. \tag{38}$$

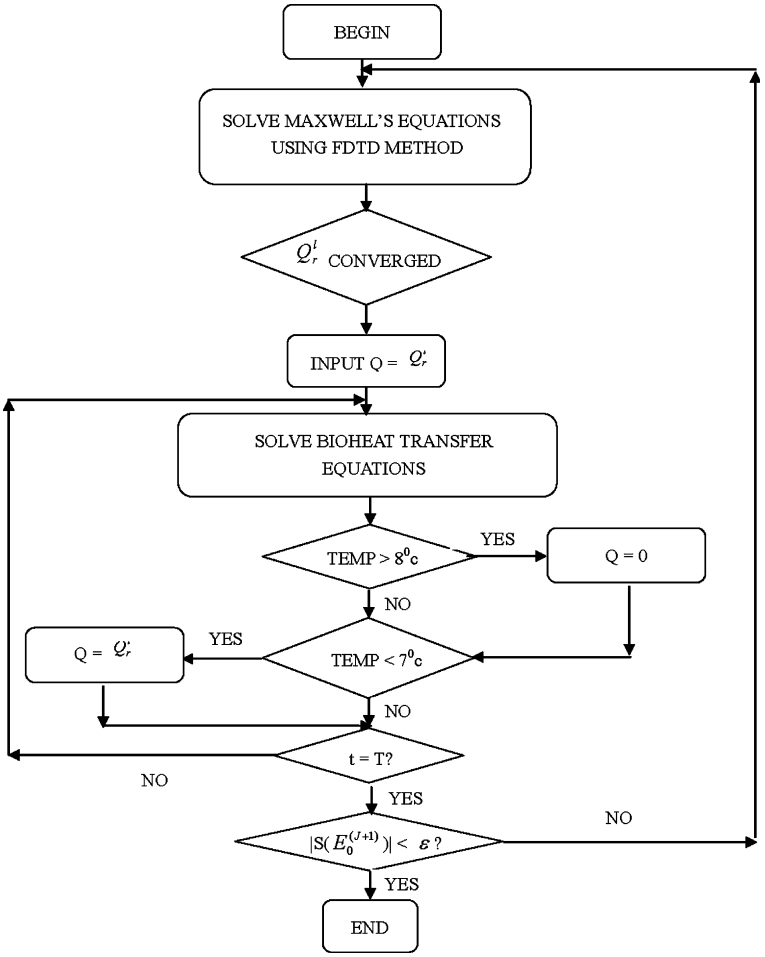

Fig. 3. Diagram of the computational algorithm.

Finally, we can employ the finite difference time domain (FDTD) method coupled with the perfectly matched layer technique [36] to obtain the EM fields. It should be pointed out that the applicability of the new FDTD solver has been tested in [37,38].

3.3. Inverse method for obtaining power intensity

To determine the amplitude E_0 of the EM wave so that an optimal temperature distribution can be obtained, we pre-specify the temperature elevations to be obtained at the center and some locations in the perimeter on the skin surface. The reason that these locations are chosen is because the hottest temperature is assumed to be around the center of skin surface, and it is insured to have the temperature in the perimeter below a certain threshold so as not to cause damage to the normal tissue, as well as the temperature could be easily measured on these locations. By guessing an initial amplitude E_0 and pre-specifying the EM wave exposure pattern, one may solve the above equations to obtain a temperature field in the entire 3D skin structure. Once the calculated temperatures, u^i_{cal}, at the given locations $(i = 0,1,\ldots,M)$ are obtained, a least squares approach can be employed to minimize the difference between the pre-specified temperature elevation θ_{pre} and the calculated temperature u_{cal} as follows:

$$S(E_0) = \sum_{i=0}^{M} (\theta^i_{\text{pre}} - u^i_{\text{cal}})^2, \quad i = 0, 1, \ldots, M. \tag{39}$$

By minimizing $S(E_0)$ in Eq. (39), a new E_0 can be calculated iteratively as follows [39]:

$$E_0^{(J+1)} = E_0^{(J)} + (X^t X + \alpha^* \mathbf{I})^{-1} X^t (\vec{\theta}_{\text{pre}} - \vec{u}_{\text{cal}}), \tag{40}$$

Table 1
Parameters for a 3D skin structure [6,22,23,31]

Parameters	Values	Parameters	Values
α (W/cm^2 °C)	0.2	k_2 (W/cm °C)	0.0052
C_1 (J/g °C)	3.6	k_3 (W/cm °C)	0.0021
C_2 (J/g °C)	3.4	$\dot{P}$ (1/s)	0.5×10^{-3}
C_3 (J/g °C)	3.06	v_1 (m/s)	0.08
C^1_{b} (J/g °C)	0	W^1_{b} (g/cm^3 s)	0
C^2_{b} (J/g °C)	4.2	W^2_{b} (g/cm^3 s)	0.0005
C^3_{b} (J/g °C)	4.2	W^3_{b} (g/cm^3 s)	0.0005
C_{B} (J/cm^3 °C)	4.134	ρ_1 (g/cm^3)	1.2
h (W/cm^2)	0.001	ρ_2 (g/cm^3)	1.2
k_1 (W/cm °C)	0.0026	ρ_3 (g/cm^3)	1

Table 2
Dielectric properties of human skin [28,40]

Parameters in the Cole–Cole expression	Values
ε_∞	4.0
σ_1	0.0002
$\Delta\varepsilon_1$	32
$\Delta\varepsilon_2$	1100
$\Delta\varepsilon_3$	0
$\Delta\varepsilon_4$	0
τ_1 (ps)	7.23
τ_2 (ns)	32.48
τ_3 (μs)	0
τ_4 (ms)	0
α_1	0.1
α_2	0.2
α_3	0
α_4	0

Table 3
Parameters used in computation

Parameters	Values	Parameters	Values
$Bi = \frac{\alpha}{k_3}$	95.23	NL^2_{b}, NW^2_{b}, (cm)	0.08
L_1 (cm)	0.008	NL^3_{b}, NW^3_{b} (cm)	0.08
L_2 (cm)	0.2	ω_1	1
L_3 (cm)	1.0	Δx (cm)	0.02
L^1_{b} (cm)	0.4	Δy (cm)	0.02
L^2_{b} (cm)	0.28	Δt (s)	0.1
L^3_{b} (cm)	0.2	δt (s)	3.3333×10^{-14}
NX, NY (cm)	0.5	Δz (cm)	0.002
NL^1_{b}, NW^1_{b} (cm)	0.1	δz (cm)	0.004

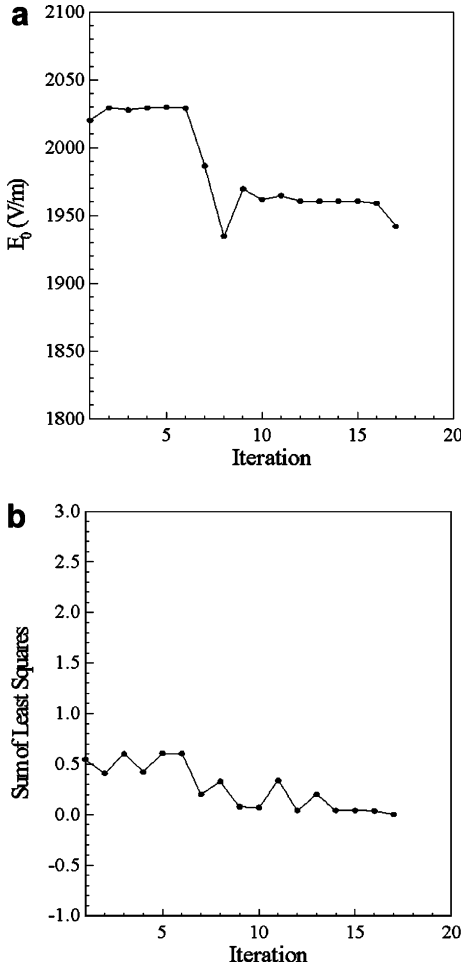

Fig. 4. Number of iterations versus (a) amplitude of the input wave E_0 and (b) sum of least squares.

where α^* is a relaxation parameter, $\mathbf{I}$ is an identity matrix, and X is the sensitivity coefficient matrix, θ_{pre} and $\vec{u}_{\text{cal}}$ are vectors consisted of θ^i_{pre} and u^i_{cal}, respectively.

3.4. Algorithm

The algorithm for calculating the required amplitude E_0 in order to obtain the pre-specified temperature elevations at given locations on the skin surface after a pre-specified EM wave exposure time can be described as follows:

Step 1. Pre-specify the temperature elevations θ^i_{pre} at given $(M+1)$ grid points $i = 0,1,\ldots,M$, on the skin surface, and pre-specify the EM wave exposure pattern. Guess an initial amplitude E_0 of the EM wave and its small increment ΔE_0.

Step 2. Run the new FDTD solver until the steady-state (pure-time harmonic) is sufficiently well approximated and the power distribution Q_r is convergent.

Step 3. Guess the wall temperature of the blood vessel θ^m_w. Obtain first the blood temperature θ^m_b, by solving Eqs. (4)–(6) using the fourth-order Runge–Kutta method. Then obtain the temperature distribution $\vec{u}_{\text{cal}}$ in the entire 3D skin structure by solving Eq. (23) with the interfacial Eqs. (24a) and (24b), and the initial and boundary conditions, Eqs. (26a)–(26e). It should be pointed out that in our computation for obtaining $\vec{u}_{\text{cal}}$, we employ a preconditioned Richardson iteration as described in [22] so that the linear system can be transferred into many tridiagonal linear systems. When the grid point (i,j,k) is in the mth level blood vessel, we let $(u_3)^n_{ijk} = (u^m_b)_{ijk}$ and hence Thomas algorithm can be used line by line along the z-direction.

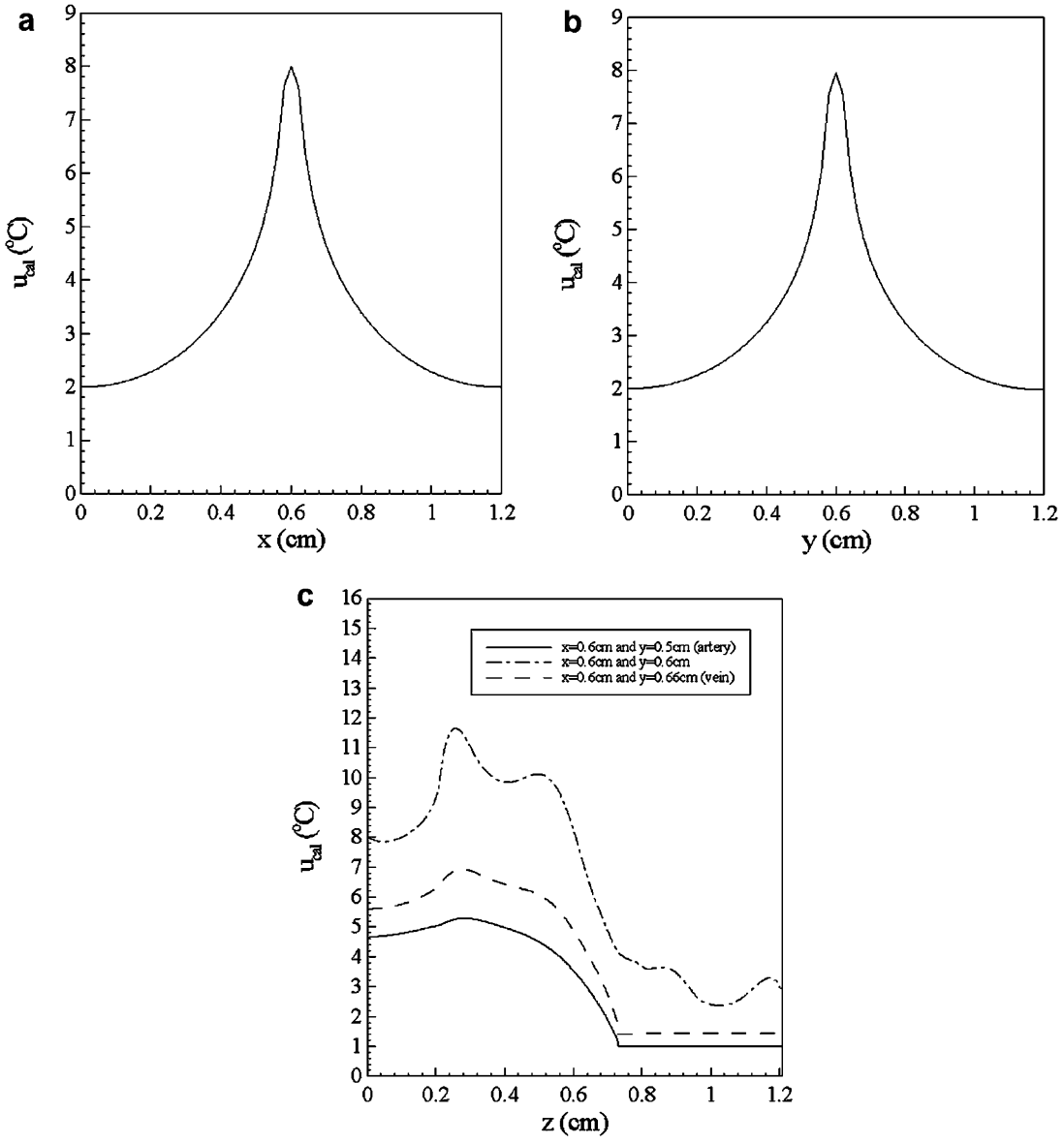

Fig. 5. Profiles of temperature elevations at $t = 400$ s: (a) in the x-direction at $y = 0.6$ cm on the skin surface, (b) in the y-direction at $x = 0.6$ cm on the skin surface, and (c) along the depth (the z-direction) at three locations.

Step 4. Update the wall temperature of the blood vessel, θ_w^m, by Eqs. (25a)–(25c).
Step 5. Repeat steps 3 and 4 until a convergent solution, $\vec{u}_{cal}$, at time level $n+1$ is obtained.
Step 6. Determine a new E_0 based on Eq. (40).

Repeat the computation until the criterion, $|S(E_0^{(J+1)})| < \varepsilon$, for convergence is satisfied.

A diagram of the algorithm can be seen in Fig. 3.

4. Numerical example

We tested our algorithm in a 3D skin structure as shown in Fig. 2, where the parameter values were chosen from Tables 1–3. The test was conducted by using the plane wave to illuminate the skin as shown in Fig. 2. The plane wave was driven at 10 GHz. The grid size, δz, in the z-direction for the new FDTD scheme was chosen to be twice as long as the grid size, Δz, used for the finite difference scheme for the bioheat transfer model. The computational domain, which includes the plane wave and was used to obtain the EM fields, was computed in a lattice with grid points $75 \times 75 \times 320$ in (x,y,z). The plane wave resides in a lattice with dimensions $3 \times 3 \times 310$ in (x,y,z) along the center line of the z-direction. On the other hand, the computational domain for obtaining the temperature distribution in the 3D skin structure was placed in a lattice with grid points $60 \times 60 \times 604$ in (x,y,z). The temperature elevation of blood at entrance was assumed to be 1 °C. The temperature elevation at the center of the skin surface was pre-specified to be 8 °C and the temperature elevation at the midpoint on each edge of the skin surface was pre-specified to be 2 °C . In our computation, we considered that there was heat convection on the skin surface ($h = 0.001$ W/cm^2 [6]).

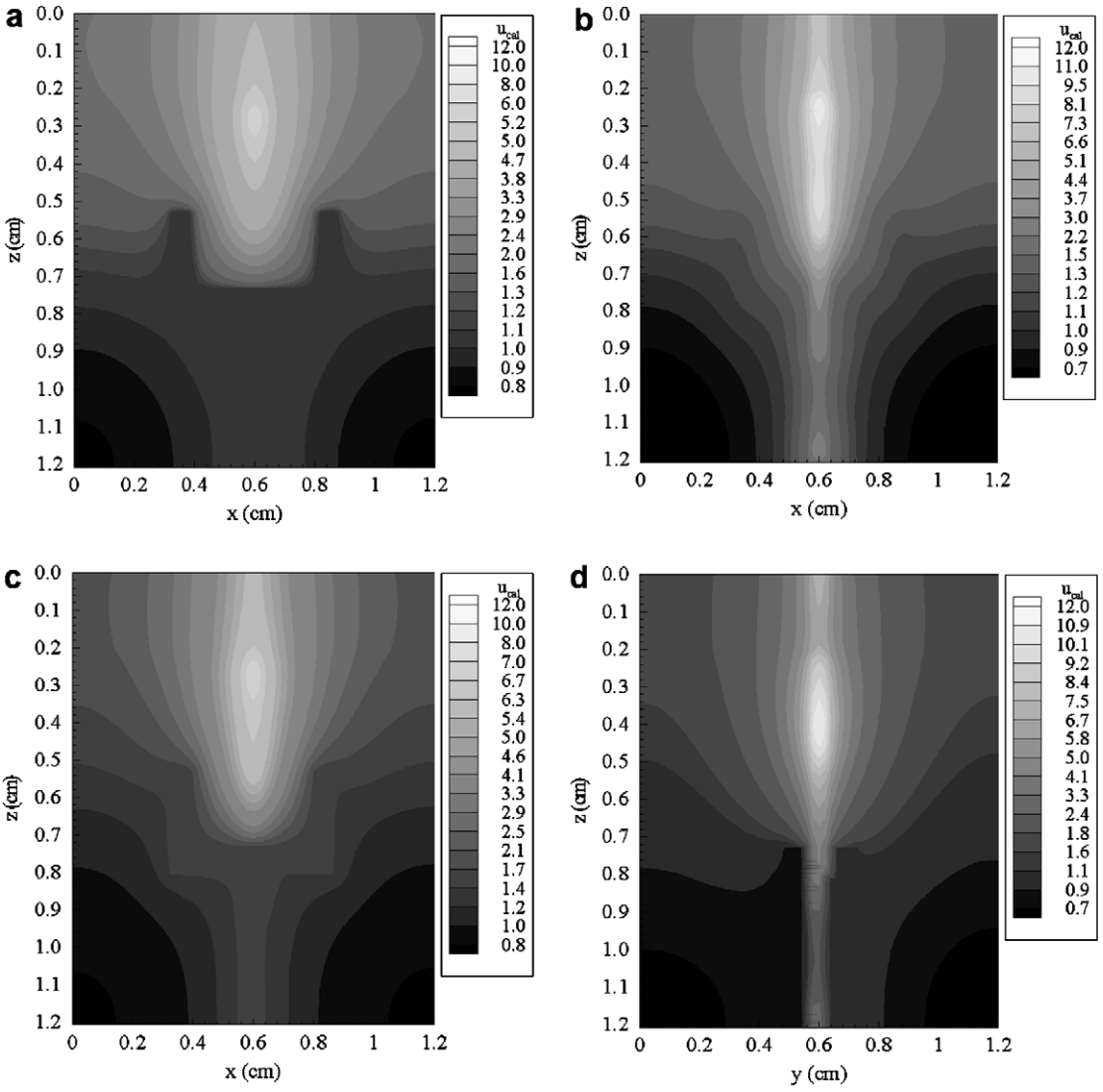

Fig. 6. Contours of the temperature elevations at $t = 400$ s in the cross-sections of the xz-plane: (a) at $y = 0.5$ cm where the artery is located, (b) at $y = 0.6$ cm, (c) at $y = 0.66$ cm where the vein is located, and the cross-section of the yz-plane at $x = 0.6$ cm.

The pattern of plane wave illumination was designed as follows: A plane wave was generated in the xy plane between the 5th grid point and the 315th grid point along the z-direction. When the temperature elevation at the center of the skin surface rose to 8 °C, the plane wave was turned off to allow heat to diffuse from the center towards the perimeter of the region. The plane wave was then turned on when the temperature elevation at the center of the skin surface decreased to 7 °C. The whole process lasted 400 s.

We started at an initial value $E_0^{(0)}$ of 2000 V/m. At the first step, $\Delta E_0^{(0)}$ was chosen to be 1% of $E_0^{(0)}$ and then $\Delta E_0^{(J)} = E^{(J)} - E^{(J-1)}$. We optimized E_0 based on the algorithm described in the previous section. The criterion for convergence is $|S(E_0^{(J+1)})| < 0.001$. Fig. 4 shows E_0 and sum of least squares versus iteration, respectively. It can be seen that E_0 is convergent to 1941.8456 V/m. Thus, we used the convergent value of E_0 to compute the temperature distribution in the 3D skin structure.

Fig. 5 shows the temperature elevation profiles at $t = 400$ s along the lines $y = 0.6$ cm and $x = 0.6$ cm on the skin surface, and along the depth (the z -direction), respectively. It can be seen that the temperature elevation at the center of the skin surface rises to 8 °C while the temperature elevation at the edge rises to 2 °C.

Fig. 6 shows the contours of the temperature elevation distributions at $t = 400$ s in these xz-cross-sections at $y = 0.5$ cm where the artery is located, at $y = 0.66$ cm where the vein is located, at $y = 0.6$ cm, and the yz-cross-section at $x = 0.6$ cm, respectively. It can be seen from this figure that the temperature profiles are symmetric in the xz-cross-section at $y = 0.6$ cm, and the temperature elevations

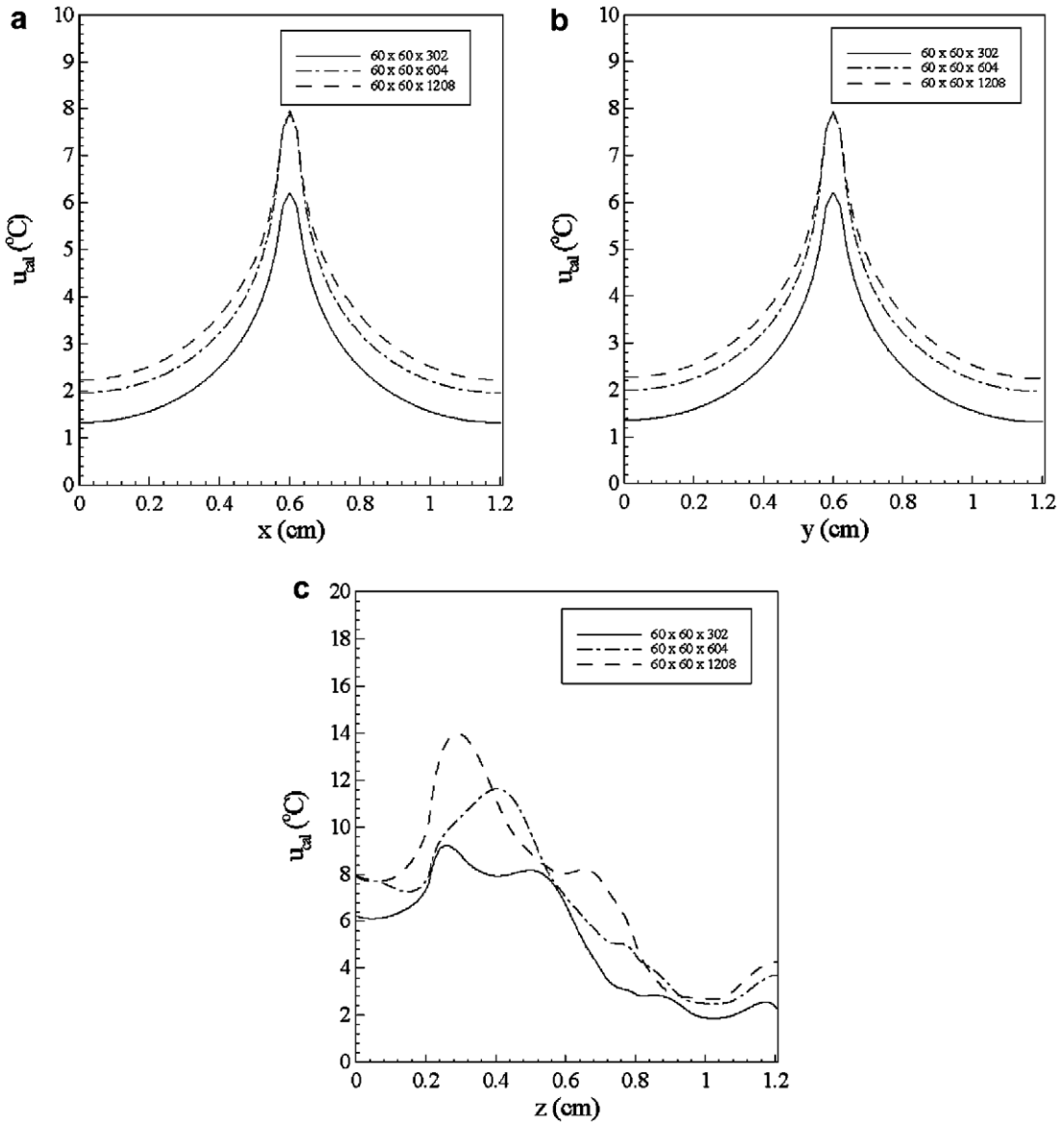

Fig. 7. Profiles of temperature elevations at $t = 400$ s: (a) in the x-direction at $y = 0.6$ cm, (b) in the y-direction at $x = 0.6$ cm on the skin surface, and (c) in the z-direction (depth) at the center of the skin surface.

around the region where the vein is located are higher than those around the region where the artery is located. This implies that the vein is carrying the heat out from the heated blood.

Fig. 7 shows the three temperature elevation profiles at $t = 400$ s (a) in the x-direction at $y = 0.6$ cm, and (b) in the y-direction at $x = 0.6$ cm on the skin surface, and (c) the depth (z-direction) at the center of the skin surface. It can be from this figure that the solution is convergent as the mesh is getting finer.

5. Conclusion

In this study we have developed a model and a numerical method for obtaining an optimal temperature distribution in a 3D triple-layered skin structure embedded with two countercurrent multi-level blood vessels and induced by electromagnetic radiation. The length and size of a blood vessel, as well as the mass flow of blood, are determined based on the constructal theory of multi-scale tree-shaped heat exchangers (for the newest review, see [41]).

The method consists of pre-specifying the temperature elevations to be obtained at the center and the edges on the skin surface, calculating the heat by solving Maxwell's equations coupled with the Cole–Cole expression, obtaining the temperature distribution by solving the 3D Pennes bioheat equation coupled with the heat transfer equations for blood, and optimizing the amplitude of the EM wave by using the least squares method. Numerical examples show that the method is applicable and efficient. Results could be useful for certain types of hyperthermia cancer treatment, such as skin cancer. Further study will focus on these cases with more complicated dendritic countercurrent multi-level blood vessels and mound-shape skin surface (tumor protuberating on the surface).

References

[1] M.H. El-Tonsy, M.M. El-Domyati, A.H. El-Din, T.E.A. Anbar, H.A. Raouf, Continuous-wave Nd:Yag laser hyperthermia: a successful modality in treatment of basal cell carcinoma, Dermatol. Online J. 10 (2006).

[2] I. Chatterjee, R.A. Adams, Finite element thermal modelling of the human body under hyperthermia treatment for cancer, Int. J. Comput. Appl. Technol. 7 (1994) 151–159.

[3] S.T. Clegg, R.B. Roemer, Predictions of three-dimensional temperature distributions during hyperthermia experiments, ASME Heat Transfer Div. 126 (1989) 29–35.

[4] N. Daikuzono, S.N. Joffe, H. Tajiri, S. Suzuki, H. Tsunekawa, M. Ohyama, Laserthermia: a computer-controlled contact Nd:YAG system for interstitial local hyperthermia, Med. Instrum. 21 (1987) 275–277.

[5] C.H. Huang, C.Y. Huang, An inverse biotechnology problem in estimating the optical diffusion and absorption coefficients of tissue, Int. J. Heat Mass Transfer 47 (2004) 447–457.

[6] H.W. Huang, Z.P. Chen, R.B. Roemer, A counter current vascular network model of heat transfer in tissues, J. Biomech. Eng. 118 (1996) 120–129.

[7] H.W. Huang, Convective thermal model formulation of a three dimensional vascular system with simplified blood flow paths: temperature distributions during hyperthermia, M.S. Thesis, University of Arizona, Tucson, AZ, 1992.

[8] C.T. Liauh, R.B. Roemer, A semilinear state and parameter estimation algorithm for inverse hyperthermia problems, J. Biomech. Eng. 115 (1993) 257–261.

[9] M.J. Piket-May, A. Taflove, W.C. Lin, D.S. Katz, V. Sathiaseelan, B.B. Mittal, Initial results for automated computational modeling of patient-specific electromagnetic hyperthermia, IEEE Trans. Biomed. Eng. 39 (1992) 226–237.

[10] E. Majchrzak, B. Mochnacki, Numerical model of heat transfer between blood vessel and biological tissue, Comput. Assisted Mech. Eng. Sci. 6 (1999) 439–447.

[11] A. Payne, M. Mattingly, R.B. Roemer, E.P. Scott, A model for a thin layer phantom with application to hyperthermia cancer therapy, Bioeng. Conf. ASME 42 (1999) 197–198.

[12] R.B. Roemer, E.G. Moros, K. Hynynen, A comparison of bioheat transfer and effective conductivity equation predictions to experimental hyperthermia data, ASME Heat Transfer Div. 126 (1989) 11–15.

[13] R.B. Roemer, Optimal power deposition in hyperthermia I. The treatment goal: the ideal temperature distribution: the role of large blood vessels, Int. J. Hyperther. 7 (1991) 317–341.

[14] S.A. Sapareto, W.C. Dewey, Thermal dose determination in cancer therapy, Int. J. Radiat. Oncol. Biol. Phys. 10 (1984) 787–800.

[15] D.M. Sullivan, Three dimensional computer simulation in deep regional hyperthermia using the finite-difference time-domain method, IEEE Trans. Microwave Theory Tech. MTT-38 (1990) 204–211.

[16] N. Tsuda, K. Kuroda, An inverse method to optimize heating conditions in RF-capacitive hyperthermia, IEEE Trans. Biomed. Eng. 43 (1996) 1029–1037.

[17] S. Waldow, P. Morrison, L. Grossweiner, Nd:YAG laser-induced hyperthermia in a mouse tumor model, Lasers Surg. Med. 8 (1988) 510–514.

[18] M.J. Wang, J.O. Naim, D.W. Rogers, R.J. Lanzafame, The effect of Nd:YAG laser-induced hyperthermia on local tumor recurrence in experimental rat mammary tumors, J. Clin. Med. Surg. 10 (1992) 265–272.

[19] L. Zhang, W. Dai, R. Nassar, A numerical modeling for optimizing laser power irradiating on a 3D triple layered cylindrical skin structure, Numer. Heat Transfer Part A 48 (2005) 21–41.

[20] L. Zhang, W. Dai, R. Nassar, A numerical method for obtaining an optimal temperature distribution in a 3d triple layered cylindrical skin structure embedded with a blood vessel, Numer. Heat Transfer Part A 49 (2006) 437–465.

[21] J. Zhou, J. Liu, Numerical study on 3D light and heat transport in biological tissues embedded with large blood vessels during laser-induced thermotherapy, Numer. Heat Transfer Part A 45 (2004) 415–449.

[22] W. Dai, A. Bejan, X. Tang, L. Zhang, R. Nassar, Optimal temperature distribution in a 3D triple layered skin structure with embedded vasculature, J. Appl. Phys. 99 (2006) 104702.

[23] X. Tang, W. Dai, R. Nassar, A. Bejan, Optimal temperature distribution in a 3D triple layered skin structure embedded with artery and vein vasculature, Numer. Heat Transfer, Part A, in press.

[24] A. Bejan, Shape and Structure, from Engineering to Nature, Cambridge University Press, Cambridge, UK, 2000.

[25] A. Bejan, The tree of convective heat streams: its thermal insulation function and the predicted $\frac{3}{4}$-power relation between body heat loss and body size, Int. J. Heat Mass Transfer 44 (2001) 699–704.

[26] A.K. da Silva, S. Lorente, A. Bejan, Constructal multi-scale tree-shaped heat exchangers, J. Appl. Phys. 96 (2004) 1709–1718.

[27] K.S. Cole, R.H. Cole, Dispersion and absorption in dielectics I. alternating current characteristics, J. Chem. Phys. 9 (1941) 341–351.

[28] S. Gabriel, R.W. Lau, C. Gabriel, The dielectric properties of biological tissues: III. Parametric models for the dielectric spectrum of tissues, Phys. Med. Biol. 41 (1996) 2271–2293.

[29] L.P. Gartner, Color Atlas of Histology, third ed., Lippincott Williams & Wilkins, Philadelphia, 2000.

[30] H.H. Pennes, Analysis of tissue and arterial temperature in the resting human forearm, J. Appl. Physiol. 1 (1948) 93–122.
[31] J. Liu, X. Chen, L.X. Xu, New thermal wave aspects on burn evaluation of skin subjected to instantaneous heating, IEEE Trans. Biomed. Eng. 46 (1999) 420–428.
[32] H.W. Huang, C.L. Chan, R.B. Roemer, Analytical solutions of Pennes bioheat transfer equation with a blood vessel, J. Biomech. Eng. 116 (1994) 208–212.
[33] C. Polk, E. Postow, CRC Handbook of Biological Effects of Electromagnetic Fields, second ed., CRC Press, Boca Raton, FL, 1995.
[34] D.D. Dincov, K.A. Parrott, K.A. Pericleous, A new computational approach to microwave heating of two-phase porous materials, Int. J. Numer. Methods Heat Fluid Flow 14 (2004) 783–802.
[35] R.L. Burden, D.J. Faires, Numerical Analysis, seventh ed., Brooks/Cole, 2001.
[36] D.M. Sullivan, Electromagnetic Simulation Using the FDTD Method, IEE, New York, 1999.
[37] S. Su, W. Dai, D. Haynie, N. Simicevic, Use of the z-transform to investigate nanopulse penetration of biological matter, J. Bioelectromagn. 26 (2005) 389–397.
[38] S. Su, W. Dai, D.T. Haynie, R. Nassar, N. Simicevic, Numerical simulation of nanopulse penetration of biological matter using the z-transform, J. Math. Modell. Algorithms 4 (2005) 99–110.
[39] M.N. Ozisik, Heat Conduction, second ed., John & Wiley, New York, 1993 (Chapter 14).
[40] H.F. Cook, The dielectric behavior of some types of human tissues at microwave frequencies, Br. J. Appl. Phys. 2 (1951) 295–300.
[41] A. Bejan, S. Lorente, Constructal theory of generation of configuration in nature and engineering, J. Appl. Phys. 100 (2006) 041301.
[42] L.T. Lorimer, The Human Body, Reader's Digest, New York, 1999.